


Maleimide-styrene-butadiene terpolymers: acrylonitrile-butadiene-styrene inspired photopolymers for additive manufacturing

Johannes Steindl,^{a†} Katharina Ehrmann,^{a†} Christian Gorsche,^a 
 Ching-Chung Huang,^a Thomas Koch,^b Patrick Steinbauer,^{a,c}
 Andreas Rohatschek,^{d,e,f} Orestis G. Andriotis,^{d,e}  Philipp J. Thurner,^{d,e,f}
 Alexander Prado-Roller,^g Jürgen Stampfl^{b,e} and Robert Liska^{a,e*} 

Abstract

The terpolymer acrylonitrile-butadiene-styrene (ABS) is a widely used thermoplastic material due to its excellent mechanical properties, especially high toughness. However, the monomer system of ABS cannot be feasibly photopolymerized due to its reactivity, opacity and monomer volatility. We show the transfer of an ABS microstructure to photopolymers via monomer systems designed to mimic ABS while remaining photopolymerizable. Acrylonitrile was substituted by more reactive and less volatile maleimides, of which the *N* substituent influences crosslinking considerably. Instead of styrene, less volatile derivatives were utilized as comonomers. Poly(butadiene) was introduced as cheap, readily available and non-volatile rubber. The resulting maleimide-styrene-poly(butadiene) networks exhibit varying microphase separations and simultaneous transparency. While optimized materials cannot quite exhibit the yield strain of hot-pressed ABS filament, their toughness partly exceeds that of ABS. Superior thermal stabilities and glass transition temperatures up to 190 °C were observed. Finally, stereolithographic printing of one tuned monomer system was conducted.

© 2021 The Authors. *Polymer International* published by John Wiley & Sons Ltd on behalf of Society of Industrial Chemistry.

Keywords: photopolymer; maleimide; styrene; poly(butadiene) rubber; additive manufacturing; microstructure

INTRODUCTION

Light-based additive manufacturing (AM) techniques have been on the rise due to their higher resolution compared with fused deposition modeling (FDM).^{1,2} Such techniques enable the facile preparation of complex shapes and simultaneously bring along new requirements for materials. Conventional photopolymers are rather brittle in bulk form due to their inhomogeneous polymer network architecture.³ Therefore, there is a need for new strategies to obtain tough photopolymers for AM.

Classical polymer toughening strategies are either refined polymerization methods for more homogeneous polymer networks or the use of additives.³ The most important polymerization method for the reduction of network inhomogeneity is thiol-ene step-growth polymerization^{4–6} but also controlled radical polymerization methods have been reported,⁷ i.e. nitroxide-mediated polymerization,^{8,9} addition-fragmentation chain transfer polymerization,^{10–13} reversible addition-fragmentation chain transfer polymerization^{14,15} and atom transfer radical polymerization^{16,17}. Within the field of additives, especially inorganic fillers but also rubbers have been explored as toughening agents in polymers. While inorganic fillers such as silica, alumina or CaCO₃ provide increased surface area and therefore increased fracture surface energy, the same mechanism can only be utilized for

* Correspondence to: R Liska, Institute for Applied Synthetic Chemistry, Technische Universität Wien, Getreidemarkt 9/163, 1060 Vienna, Austria. E-mail: robert.liska@tuwien.ac.at

† These authors contributed equally to this article.

a Institute for Applied Synthetic Chemistry, Technische Universität Wien, Vienna, Austria

b Institute of Materials Science and Technology, Technische Universität Wien, Vienna, Austria

c Christian Doppler Laboratory for Advanced Polymers for Biomaterials and 3D Printing, Technische Universität Wien, Vienna, Austria

d Institute of Lightweight Design and Structural Biomechanics, Technische Universität Wien, Vienna, Austria

e Austrian Cluster for Tissue Regeneration, Vienna, Austria

f Biointerface Doctorate School, TU Wien, Vienna, Austria

g Department of Inorganic Chemistry – Functional Materials, Faculty of Chemistry, University of Vienna, Vienna, Austria

rubbers if applied as core-shell particles that are labor and cost intensive in manufacturing.^{3,18–20} Another strategy to integrate rubbers as toughening components is the use of low molecular weight liquid rubbers with reactive end groups^{21–23} instead of high molecular weight rubbers, which ultimately lead to high formulation viscosities. Using high molecular weight components to produce polymer networks with wider meshes has only recently become interesting for photopolymers intended for AM due to the development of hot lithography.^{24,25}

One of the most prominent examples for tough engineering plastics is the terpolymer acrylonitrile-butadiene-styrene (ABS),²⁶ which utilizes rubber toughening. The microphase separated morphology of ABS consists of soft poly(butadiene) domains covalently embedded in a hard and rigid poly(styrene-co-acrylonitrile) matrix. It yields a very tough material while maintaining other important properties like stiffness or heat resistance.²⁷ The favorable chemical and thermomechanical properties within a broad application range (-20 to 80 °C), good processability (injection molding, extrusion) and versatile post-processing (e.g. bonding, welding, electroplating, printing) make ABS copolymers interesting for many purposes, e.g. household and consumer goods, pipes, toys, automotive and electrical applications, and filaments for FDM.^{26,28,29} However, the reactivity of these monomers during photopolymerization is at best modest due to quenching of the excited state of most photoinitiators and the opaque appearance of ABS copolymers.

A photopolymerizable alternative to ABS would be very interesting for countless applications and especially AM. Here, we have developed a photopolymerizable monomer system to produce polymer networks, which contain covalently bound polybutadiene as a toughening component and exhibit microphase separation in analogy to ABS copolymers. The poly(butadiene)-based toughening component was introduced into the photopolymer as a cheap, readily available and non-volatile rubber ($M_n = 180$ kDa). To achieve feasible photopolymerization, substitution of the acrylonitrile component with more reactive and less volatile monomers was necessary. Since maleimides are known to copolymerize well with styrene due to their activated (electron-poor) and additionally ring-strained double bond, various maleimides were chosen as substitutes.^{30–33} While the electron-rich double bond in styrene exhibits sufficient reactivity for photopolymerization, its volatility remains problematic. Therefore, substituted versions of styrene were examined as suitable comonomers. Polymerization speed and conversion were investigated for all formulations. Interaction of poly(butadiene) with the maleimide-styrene matrix was observed and the mechanism behind it was elucidated. To determine potential fields of applications, we assessed the thermal and mechanical performance as well as the potential for phase separation of the resulting materials.

EXPERIMENTAL

Materials

The chemicals vinylbenzyl chloride (mixture of meta and para substituted isomers, Sigma-Aldrich, St. Louis, Missouri, United States), sodium hydride (TCI Chemicals, Tokyo, Japan), fenchol (Sigma-Aldrich), ammonium chloride (Carl Roth, Karlsruhe, Germany), anhydrous sodium sulfate (VWR, Radnor, Pennsylvania, United States), silica (Merck, Kenilworth, New Jersey, United States), maleic anhydride (Sigma-Aldrich), menthyl anthranilate (meradimate, Sigma-Aldrich), 2-ethyl-1-hexylamine (abcr, Karlsruhe, Germany), anhydrous sodium acetate (Sigma-Aldrich),

sodium bicarbonate (Donau Chemie, Vienna, Austria), phenothiazine (Sigma-Aldrich), acetic anhydride (Alfa Aesar, Haverhill, Massachusetts, United States), light absorber Sudan Yellow (Sigma-Aldrich), benzophenone (Sigma Aldrich) and *N*-methyl-diethanolamine (Sigma Aldrich) were purchased and used for synthesis/experiments without further purification unless mentioned otherwise. Furthermore, the monomers isobornyl methacrylate (IBMA) (TCI Chemicals), *N*-propyl maleimide (PrMI) (abcr), 4-*tert*-butylstyrene (tBuSt) (abcr) and *N*-cyclohexyl maleimide (CHMI) (TCI Chemicals) were obtained from the respective commercial sources and used directly. The photoinitiators Ivocerin and ethyl (2,4,6-trimethylbenzoyl) phenyl (TPO-L) and poly(butadiene) rubber (Buna CB 24) were kindly gifted by Ivoclar Vivadent (Schaan, Liechtenstein), Lambson (Wetherby, UK) and Arlanexo (The Hague, Netherlands), respectively. Commercial grade solvents (dry dimethylformamide, Sigma-Aldrich; CHCl_3 , Acros; diethyl ether, dichloromethane, petrol ether and ethyl acetate, Donau Chemie; CDCl_3 , deuterated dimethyl sulfoxide, Eurisotop, Saint-Aubin, France) were used as purchased. ABS filament for FDM was purchased from RSpro (Barcelona, Spain, ABS@df, black, 1.75 mm, polymer composition according to manufacturer >98% styrene-acrylonitrile-butadiene copolymer (CAS: 9003-56-9), <0.1% styrene (CAS: 100-42-5)).

General characterization methods

A Bruker Avance DRX-400 was used for NMR spectroscopy at 400 MHz for ^1H (^{13}C 100 MHz) and chemical shifts were reported in parts per million. They were referenced to the solvent residual peak for ^1H (CDCl_3 ; $\delta\text{H} = 7.26$ ppm) and ^{13}C (CDCl_3 ; $\delta\text{C} = 77.16$ ppm). To measure the total irradiation intensities at the position of the samples, an Ocean Optics USB 2000+ spectrometer was used. Molecular weights were measured at 40 °C on a Malvern Viscotek GPCmax VE2001 system equipped with an RI detector (VE3850), a Malvern Viscotek SEC-MALS 9 detector and a Malvern Viscotek TDA. Three columns from Waters GmbH (Waters Styragel HR 0.5 THF, Waters Styragel HR 3 THF and Waters Styragel HR 4 THF) were used with dry tetrahydrofuran (THF) as the mobile phase (flow rate of 1 mL min⁻¹). The samples were dissolved in dry THF and filtered through a 0.2 μm polytetrafluoroethylene disposable syringe filter. The injection volume was 100 μL . Calibration was conducted with polystyrene standards (M_n range between 370 Da and 177 kDa). The software OmniSEC 5.12 was used for data acquisition and analysis of number-average (M_n), weight-average molecular weight (M_w) and molar mass dispersity D (M_w/M_n).

Preparation of resin formulations and polymer specimens

All preparation steps and handling of photopolymerizable resins were carried out in an orange-light laboratory to prevent photopolymerization. The photoinitiator TPO-L was used with a concentration of 0.2 wt% in all formulations. The resin for 3D printing was prepared with 1 wt% Ivocerin to fit the photoinitiator absorption spectrum and irradiation wavelength of 460 nm. Additionally, 0.1 wt% light absorber (Sudan Yellow 177) was added to the resin for printing. All resins were mixed in an ultrasonic bath until a homogeneous formulation was obtained. The formulations were used for storage stability tests, photo-DSC and real-time near infrared photorheology (RT-NIR-photorheology). Polymer specimens for swellability (discs 4 mm diameter, 2 mm thickness), dynamic mechanical thermal analysis (DMTA) ($5 \times 2 \times 40$ mm³), tensile tests (ISO 527, specimen shape 5B), impact resistance ($10 \times 4 \times 15$ mm³) and AFM/small angle X-ray scattering (SAXS) (cuttings from tensile test specimens) were obtained by curing these

formulations in silicon molds in a Uvitron International Intelli-Ray 600 (600 W Hg bulb, broadband UV radiation, 125 mW cm⁻² in UVA, 125 mW cm⁻² in the visible region) for 5 min on each side. Finally, the polymer samples were sanded to ensure a uniform shape. ABS specimens were prepared from dry filament (70 °C, 24 h) by compression molding at 230 °C with stepwise pressure increase from 0.45 to 2.20 MPa. Specimens were die-cut from a 2 mm thick plate for tensile testing and cut from a 4 mm thick plate and ground for Dynstat experiments. For grinding, SiC paper with 400–1200 grit was purchased from Bühler.

Photo-DSC

An Omniscience light source (Hg broadband, filtered UV light 320–500 nm, 1 W cm⁻² at the exit of the light guide corresponding to ca 20 mW cm⁻² on the surface of the sample) coupled with a Netzsch DSC 204 F1 was used for photo-DSC measurements. All samples were weighed into aluminium pans (10 ± 1 mg) and were irradiated twice for 5 min at 25 °C under an inert atmosphere (N₂ flow rate of 20 mL min⁻¹). The second irradiation period of 5 min was performed to eliminate the influence of heat effects originating from light absorption of the sample or the aluminium pan. Triplicate measurements were conducted for each sample formulation.

RT-NIR-photorheology

All experiments were performed on an RT-NIR-photorheology device with a Bruker Vertex 80 FTIR spectrometer and an Anton Paar MCR302 WESP rheometer, which is equipped with a PP-25 steel measurement system and a P-PTD 200/GL Peltier element.³⁴ The temperature at the optical quartz rheometer plate was set to 25 °C and 140 µL of the sample were placed on it with an Eppendorf pipette. Afterwards, the measurement gap was set to 200 µm. The respective samples were measured via NIR spectroscopy and analyzed by rheology before the start of UV irradiation. The formulations were oscillated with a strain of 1% and a frequency of 1 Hz. The samples were irradiated with UV light from below the optical plate to start the reaction using an Exfo OmniCureTM 2000 with a broadband Hg lamp (300 s, 320–500 nm, 10 mW cm⁻² on the surface of the sample). The curing reaction was monitored by recording time-resolved NIR spectra as well as the storage modulus G' and loss modulus G'' of the sample. The gel point of each photopolymerization reaction was obtained from the intersection of storage and loss moduli ($G'/G'' = 1$). The chemical conversion (double bond conversion, DBC) was determined by recording single IR spectra with a time interval of ca 0.25 s using the software OPUS 7.0. The relevant peak area for the reactive double bond moieties (i.e. overtones at 6080–6250 cm⁻¹) was evaluated. The ratio of the peak areas before irradiation and at the end of the measurement gives the DBC. The conversion at the gel point DBC_{gel} and final DBC (DBC_{end}) were obtained from this plot. All measurements were performed in triplicate.

Swellability

Disc-shaped polymer specimens (diameter 4 mm, thickness 2 mm, ca 35 mg) were submerged in CHCl₃ if not indicated otherwise and stored in ambient conditions for 7 days. The solvent was replaced after 3 days. The polymers were dried using a paper towel and weighed. Afterwards, the discs were placed in a vacuum oven at 60 °C and dried until their weight remained constant. All measurements were performed in triplicate.

Dynamic mechanical thermal analysis

An Anton Paar MCR 301 with a CTD 450 oven and an SRF 12 measuring system was used for DMTA measurements. The experiments were executed in torsion mode with a frequency of 1 Hz, strain of 0.1%, constant normal force of -1 N and a temperature ramp of 2 °C min⁻¹ from -130 to 250 °C. The software Rheo-plus/32 V3.40 from Anton Paar was used for data recording.

Tensile testing

A Zwick Z050 testing machine equipped with a 1 kN load cell was used for tensile tests according to ISO 527. Five dumbbell specimens (shape 5B) were tested for each formulation. The respective specimens were strained with a crosshead speed of 5 mm min⁻¹. A stress–strain plot was recorded.

Dynstat impact resistance measurements

Dynstat impact testing was executed according to DIN 51230. The polymer specimens were broken with a 2 J hammer. Four specimens were tested for each sample and the acquired value was normalized to the width and thickness of the respective specimen. The impact resistance is determined by the ratio of work required to break the specimen in kilojoules to the cross-section of the sample in square meters.

Atomic force microscopy

AFM experiments were performed on a NanoWizard® ULTRA SpeedA AFM system (JPK Instruments AG, Berlin) equipped with an inverted optical microscope (Axio Observer D1, ZEISS). Nano-mechanical assessment was performed via AFM cantilever-based nanoindentation experiments using a 4XC-NN-C rectangular cantilever (spring constant determined as 3.7 N m⁻¹; µMasch, OPUS™) equipped with a sharp tip (nominal tip radius ca 7 nm). The cantilever spring constant was calibrated by the thermal noise method³⁵ and the deflection sensitivity for a setpoint force of 20 nN was calibrated by an iterative approach of several force maps consisting of 16 force measurements each. All calibration measurements were performed on glass.³⁶ A 5 × 5 µm² region of interest was scanned in Quantitative Imaging mode (QI™, JPK) with a maximum applied force of 20 nN and spatial resolution of 256 × 256 pixels to spatially resolve the indentation modulus. This results in force indentation curves mapped over the region of interest, which were analyzed to obtain the indentation modulus. The indentation modulus was calculated by employing a Hertz–Sneddon analysis method³⁷ and assuming the tip shape to be a paraboloid with a tip radius of 7 nm. The sample surface was prepared from one end of a cured tensile test specimen by cutting the clamping area in half with a scalpel and immobilizing the sample on a glass surface. Surface roughness after cutting was too high for direct measurement; therefore the sample was ground.

Small angle X-ray scattering

SAXS data acquisition was performed on a Xenocs Nano-inXider 2.3 device in transmission geometry using Cu Kα radiation (1.54 Å) in very high resolution mode, with a PILATUS3 2x100K detector (Dectris) situated at 935 mm from the sample, for merged 500 min exposure time. Details regarding data processing can be found in the Supplementary information.

Dynamic light processing (DLP) printing

The 3D printing experiments were performed on a self-made DLP printer equipped with a diamond-WXGA light engine (460 nm, 6 mW cm⁻² intensity at the sample surface).²⁵ Each layer of

50 μm thickness was irradiated for 40 s at room temperature and at a contact pressure of 60 N.

RESULTS AND DISCUSSION

Copolymerization of maleimides and styrenes

Four equimolar formulations containing one maleimide and one styrene were investigated with regard to their copolymerization behavior (MIS_t1–4). Four maleimides with varying *N* substituents were chosen to investigate the effect of varying reactivity and steric hindrance on the final polymer: PrMI, *N*-(2-ethylhexyl)maleimide (EHMI), CHMI and *N*-meradimatemaleimide (MMI) (Scheme 1). While PrMI and CHMI are commercially available, EHMI and MMI were synthesized (procedures described in the Supplementary information). To compare the monomers' properties with a well-known photopolymerizable reference monomer, IBMA was analyzed additionally.

MIS_t1 contains PrMI and tBuSt (Scheme 1), which are both rather volatile for applications at elevated temperatures

(Table S1). However, the high reactivity of the monomers is sufficient for room temperature curing and therefore investigation of these monomers may be interesting due to their low steric demand, which may impact the resulting mechanical properties. MIS_t2–4 all utilize styrene-based FES_t (a mixture of 1,3,3-trimethyl-2-((3-vinylbenzyl)oxy)bicyclo[2.2.1]heptane and 1,3,3-trimethyl-2-((4-vinylbenzyl)oxy)bicyclo[2.2.1]heptane) with varying *N*-substituted maleimides, all of which exhibit low volatility and higher steric hindrance (Scheme 1). The selection of maleimides covers aliphatic and aromatic substituents, which were expected to impact reactivity.

All MIS_t formulations could be stored for at least 4 months in the dark at room temperature under air without any sign of polymerization with the exception of MIS_t1 which showed a storage stability of only 3 days. This suggests higher reactivity of MIS_t1, which was investigated further via photo-DSC and RT-NIR-photorheology experiments.

Since self-initiation of maleimides or MIS_t charge-transfer complexes has been reported in the literature,^{30,38–40} a photo-DSC

| | MIS _t 1 | MIS _t 2 | MIS _t 3 | MIS _t 4 |
|--------------------------------|--------------------|----------------------|--------------------|--------------------|
| Maleimide (MI) | | | | |
| | PrMI | EHMI | CHMI | MMI |
| Styrene (St) | tBuSt | FES _t | | |
| (Poly)butadiene Rubber (BR) | BR | | | |

Scheme 1. Overview of formulation components for MIS_t1–4

Table 1. Summary of photo-DSC data obtained for all monomers and formulations: polymerization times at which the peak maximum is reached (t_{\max}) and at which 95% of final conversion is reached ($t_{95\%}$), polymerization heat (ΔH_{pol}), double bond conversion of maleimide or methacrylate ($\text{DBC}_{\text{MI/MA}}$), double bond conversion of styrene comonomer (DBC_{St}), number-average molecular weight (M_n) and molar mass dispersity (\mathcal{D})

| Monomer or formulation ^a | t_{\max} / s | $t_{95\%}$ / s | ΔH_{pol} / J g ⁻¹ | $\text{DBC}_{\text{MI/MA}}$ / % | DBC_{St} / % | M_n / kDa | \mathcal{D} |
|-------------------------------------|----------------|----------------|---|---------------------------------|------------------------------|-------------|---------------|
| MIS1_0 | 21.1 | 41.0 | 372 | n.d. (insoluble) | | | |
| MIS1_10 | 18.7 | 63.1 | 307 | n.d. (insoluble) | | | |
| MIS1_20 | 14.3 | 57.9 | 288 | n.d. (insoluble) | | | |
| MIS2_0 | 17.6 | 32.9 | 303 | n.d. (insoluble) | | | |
| MIS2_10 | 17.3 | 38.0 | 274 | n.d. (insoluble) | | | |
| MIS2_20 | 16.9 | 42.9 | 264 | n.d. (insoluble) | | | |
| MIS3_0 ^b | 12.2 | 28.4 | 312 | n.d. (insoluble) | | | |
| MIS3_10 ^b | 11.8 | 32.4 | 291 | n.d. (insoluble) | | | |
| MIS3_20 ^b | 10.8 | 36.4 | 276 | n.d. (insoluble) | | | |
| MIS4_0 | 14.1 | 63.8 | 142 | 62 | 61 | 100.0 | 6.9 |
| MIS4_10 | 21.5 | 92.8 | 134 | n.d. (insoluble) | | | |
| MIS4_20 | 14.0 | 98.3 | 123 | n.d. (insoluble) | | | |
| IBMA_0 | 11.9 | 176.9 | 95 | 47 | – | 37.4 | 6.6 |
| IBMA_10 | 35.4 | 91.9 | 101 | 52 | – | 38.1 | 8.7 |
| IBMA_20 | 22.0 | 92.6 | 88 | 53 | – | 43.4 | 8.1 |

^a Each formulation contains equimolar amounts of maleimide (MI) and styrene (St) monomers, where the numbers 1–4 characterize the MI/St combination according to Scheme 1; the number at the end describes the content of poly(butadiene) rubber (BR, 180 kDa) in wt%, i.e. 0 wt%, 10 wt% or 20 wt%.

^b Data obtained from measurements at 80 °C due to the insolubility of solid CHMI in FES1 at room temperature.

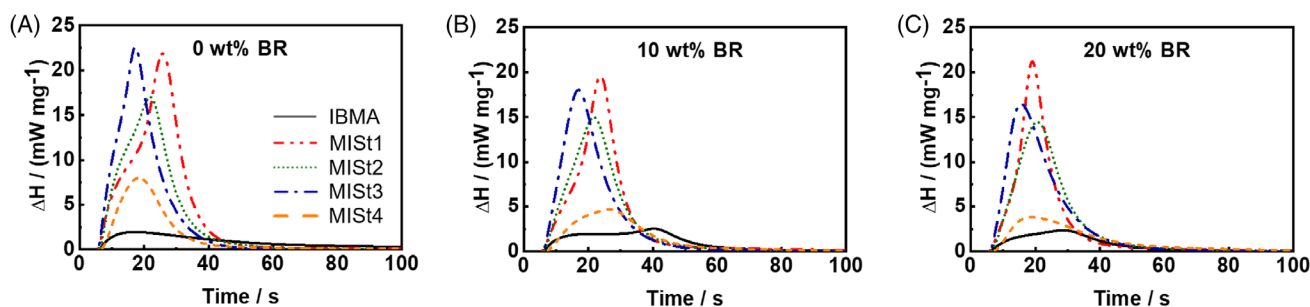


Figure 1. Photo-DSC curves of MIS1–4 formulations (for formulation components see Scheme 1) and IBMA with 0 wt% (A), 10 wt% (B) and 20 wt% (C) poly(butadiene) rubber (BR) content.

analysis at 320–500 nm was conducted for MIS1 in the absence and presence of benzophenone, alone or in combination with *N*-methyldiethanolamine as co-initiator. No photopolymerization reactions were observed and therefore the possibility of self-initiation was eliminated under the applied irradiation conditions.

The reactivity of MIS1–4 with 0.2 wt% TPO-L was also determined by photo-DSC at 25 °C to confirm whether light-stimulated initiation is applicable for these systems (Table 1, grey entries, Fig. 1(A)). MIS3 could only be homogenized at 80 °C due to the low solubility of CHMI in FES1 and was therefore examined at 80 °C. Thus, MIS3 data cannot be compared directly with the other formulations. All formulations became solid upon curing and oxygen inhibition was never observed as the sample surfaces were non-sticky. Both the polymerization heat and time of MIS1 indeed indicate high reactivity and fast polymerization of this less sterically hindered system as expected. MIS2, which also contains a flexible aliphatic residue, shows similarly high reactivity and even faster polymerization speed causing occurrence of the Trommsdorff effect, while aromatically substituted MIS4 exhibits moderate reactivity. This is in agreement with the lower

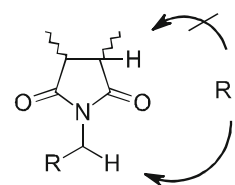


Figure 2. Two possible H-abstraction sites at a substituted maleimide.

reactivity of aromatic maleimides due to the lack of labile protons adjacent to the maleimide group as reported in the literature^{30,41} and may be enhanced in photopolymerized formulations due to light absorption of the aromatic maleimide. Even though the reactivity of cycloaliphatically substituted MIS3 cannot be compared directly, its polymerization heat and time do not counteract the trend that aliphatic substituents are more reactive. Compared to all MIS1 systems, the polymerization reaction proceeds faster for IBMA than for any MIS1 formulation. However, longer overall polymerization time and

Table 2. Swellability (*s*) and gel fraction (*g*) data for polymers pMIS_t1–4 in CHCl₃ without and with 10 or 20 wt% poly(butadiene) rubber (BR), calculated from Eqns (1) and (2), respectively

| Polymer ^a | Swellability <i>s</i> / % | Gel fraction <i>g</i> / % |
|------------------------|---------------------------|---------------------------|
| pMIS _t 1_0 | 1650 | 87.5 |
| pMIS _t 1_10 | 1210 | 88.6 |
| pMIS _t 1_20 | 1110 | 92.5 |
| pMIS _t 2_0 | 15 980 | 22.7 |
| pMIS _t 2_10 | 1770 | 81.9 |
| pMIS _t 2_20 | 1140 | 91.9 |
| pMIS _t 3_0 | 28 740 | 18.0 |
| pMIS _t 3_10 | 1240 | 78.1 |
| pMIS _t 3_20 | 900 | 85.1 |
| pMIS _t 4_0 | _b | 0.0 ^b |
| pMIS _t 4_10 | 1840 | 10.6 |
| pMIS _t 4_20 | 1590 | 53.0 |

^a Each polymer contains equimolar amounts of maleimide (MI) and styrene (St) monomers, where the numbers 1–4 characterize the MI/St combination according to Scheme 1; the number at the end describes the content of poly(butadiene) rubber (BR, 180 kDa) in wt%, i.e. 0 wt%, 10 wt% or 20 wt%.
^b Fully soluble.

lower final conversion prove that IBMA does not polymerize nearly as efficiently as MIS_t formulations.

Interestingly, cured MIS_t formulations were not soluble anymore with the exception of MIS_t4. Neither apolar CHCl₃ nor polar ethanol was capable of dissolving polymerized MIS_t1–3, even after prolonged exposure, while polymerized MIS_t4 dissolved readily. This suggests crosslinking of the formulations MIS_t1–3 due to H abstraction from the N-adjacent methylene group as indicated in Fig. 2, which cannot occur in MIS_t4. To gain more insights into crosslinking behavior, swellability (*s*) and gel fraction (*g*) of the polymers were investigated by determining their initial

weight (*m*₀), swollen weight after incubation in CHCl₃ at room temperature for 7 days (*m*_s) and weight after drying (*m*_d) and subsequent calculations according to

$$s = \frac{m_s}{m_d} \bar{n} 100 \quad (1)$$

$$g = \frac{m_d}{m_0} \bar{n} 100 \quad (2)$$

(Table 2, grey entries). The results obtained suggest that these properties depend on steric hindrance of the *N* substituent in maleimide. More bulky substituents lead to higher swellability and gel fraction. This can be explained by lower crosslinking densities for copolymers containing sterically more demanding components.

Due to the crosslinking behavior of MIS_t formulations, the determination of DBC via NMR and molecular weight via gel permeation chromatography of samples cured during photo-DSC experiments was only possible for pMIS_t4 (Table 1). Therefore, DBC was additionally calculated from NIR signals obtained before (*A*₀) and during (A) RT-NIR-photorheology for all formulations:

$$\text{DBC} = 100 - \frac{A}{A_0} \bar{n} 100 \quad (3)$$

(Table 3, grey entries, Fig. 3(A)). Again, all experiments were conducted at 25 °C with the exception of MIS_t3, which was measured at 80 °C and is therefore not directly comparable to the other measurements. Due to the overlap of maleimide and styrene double bonds (6100 and 6130 cm⁻¹, respectively), DBC is determined as an overall value and is not given separately for the monomers. However, alternating copolymerization of maleimides and styrenes is well known from the literature^{30,33,42} and is also evident for MIS_t4 in this study, for which the DBCs obtained from photo-DSC and from RT-NIR-photorheology are in excellent agreement despite varying irradiation intensities during the two analyses. Compared to the reference IBMA, higher final DBCs were reached

Table 3. Summary of RT-NIR-photorheology data obtained: time until gelation (*t*_{gp}), double bond conversion at gelation point (DBC_{gp}), time until 95% conversion (*t*_{95%}), final double bond conversion (DBC_{end}) and shrinkage force (*F*_{s,DBCend})

| Formulation ^a | <i>t</i> _{gp} / s | DBC _{gp} / % | <i>t</i> _{95%} / s | DBC _{end} / % | <i>F</i> _{s,DBCend} / N |
|--------------------------|----------------------------|-----------------------|-----------------------------|------------------------|----------------------------------|
| MIS _t 1_0 | 31 | 36 | 101 | 88 | 22.9 |
| MIS _t 1_10 | 21 | 17 | 109 | 92 | 14.6 |
| MIS _t 1_20 | 19 | 15 | 141 | 95 | 15.5 |
| MIS _t 2_0 | 45 | 73 | 91 | 95 | 18.5 |
| MIS _t 2_10 | 36 | 33 | 107 | 95 | 19.2 |
| MIS _t 2_20 | 30 | 27 | 103 | 97 | 19.9 |
| MIS _t 3_0 | 34 | 79 | 79 | 93 | 11.4 |
| MIS _t 3_10 | 18 | 24 | 67 | 95 | 20.4 |
| MIS _t 3_20 | 16 | 24 | 64 | 97 | 20.2 |
| MIS _t 4_0 | _b | _b | 201 | 67 | 9.0 |
| MIS _t 4_10 | 45 | 27 | 203 | 81 | 11.8 |
| MIS _t 4_20 | 43 | 22 | 195 | 83 | 12.4 |
| IBMA_0 | 121 | 55 | 167 | 60 | 9.1 |
| IBMA_10 | 79 | 43 | 211 | 59 | 10.5 |
| IBMA_20 | 47 | 30 | 225 | 60 | 11.8 |

^a Each formulation contains equimolar amounts of maleimide (MI) and styrene (St) monomers, where the numbers 1–4 characterize the MI/St combination according to Scheme 1; the number at the end describes the content of poly(butadiene) rubber (BR, 180 kDa) in wt%, i.e. 0 wt%, 10 wt% or 20 wt%.

^b Not gelled.

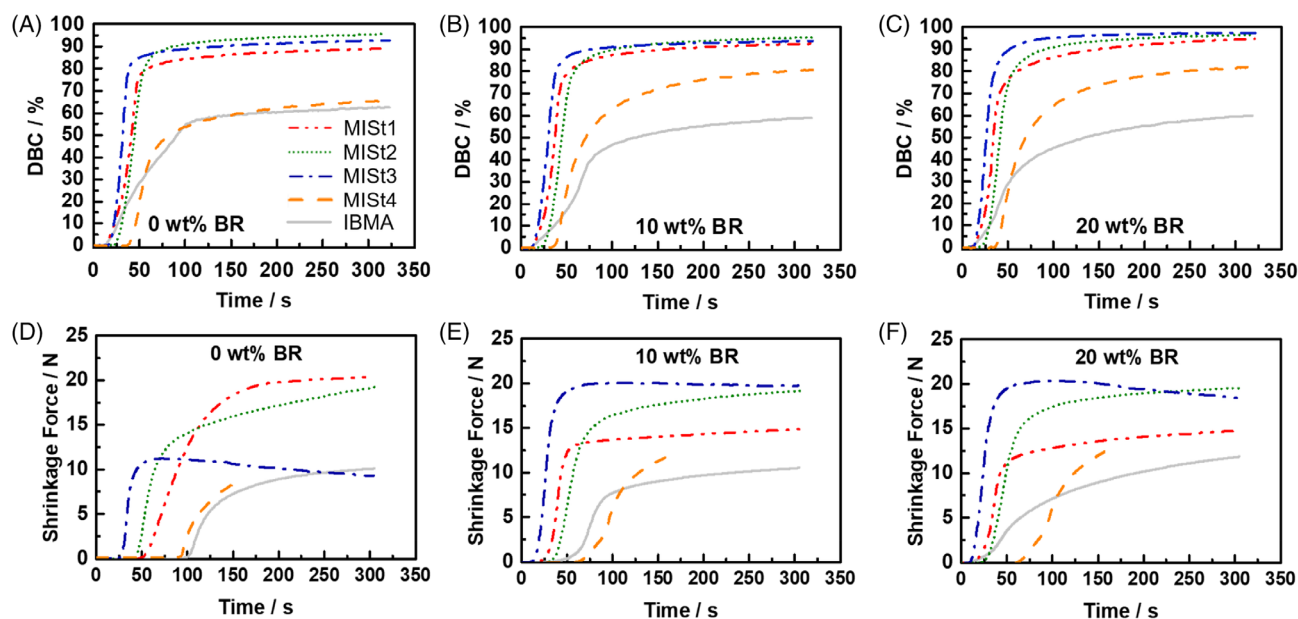


Figure 3. Double bond conversion (DBC) ((A)–(C)) and shrinkage force (F_s) ((D)–(F)) determined by photo-rheology for 0–20 wt% poly(butadiene) rubber (BR) content.

and as suspected DBCs correlated with swelling and gel fractions. Times until gelation and overall reaction times of MIST formulations containing aliphatic maleimides were faster than for IBMA while MIST4, which contains the aromatic MMI, reacted more slowly and did not gel due to low conversion caused by lower reactivity^{30,41} and higher absorbance of aromatic maleimides. This renders MIST4 an unlikely candidate as a potential material solution for the intended ABS-inspired material approach for AM. The degree of steric hindrance influenced DBC at the gel point (DBC_{gp}) significantly. While DBC_{gp} was still low for MIST1, DBC of MIST2 and MIST3 was much closer to the final DBC. Likewise, shrinkage force, which is determined by the absolute value of the normal force on the oscillating plate during rheology measurements, correlates with the degree of steric hindrance at DBC_{end} due to the influence of the residue on DBC_{end} (Table 3, grey entries, Figs 3(D)–3(F)). Sterically flexible MIST1 exhibited the highest shrinkage force at DBC_{end} (20.2 N) and the sterically most demanding MIST4 exhibited a shrinkage force comparable to IBMA with only 59% conversion (9.1 N).

Toughening with poly(butadiene) rubber: reactivity and crosslinking behavior

Finally, cheap and readily available poly(butadiene) rubber (BR) (180 kDa, >96% *cis*-1,4-poly(butadiene), Scheme Scheme 1) was added to the system to increase the toughness of the cured material. MIST1–4 formulations containing 0, 10 and 20 wt% BR were investigated for the impact of rubber addition on the curing process due to alterations in viscosity, monomer concentration and potential crosslinking via double bonds of BR. These formulations and the resulting materials were also investigated via photo-DSC, RT-NIR-photoreology, viscosity and swellability. Amounts above 20 wt% of BR could not be dissolved in the liquid components of the system anymore and were therefore not tested.

Reactivity investigations by photo-DSC showed that maximum polymerization heats were reached faster but curing time for 95% conversion increased with increasing amounts of BR (MIST_0 to MIST_20) for all MI/St combinations (MIST1–4, Table 1,

Figs 1(A)–1(C)). This can be explained by higher viscosities of formulations with higher rubber content as confirmed by rheology and dilution of double bonds with BR. Polymerization heat also drops with increasing BR content due to lower double bond concentrations. If there were no reaction between the MIST and BR phase, the drop in polymerization heat was expected to be 10% for MIST formulations containing 10 wt% BR and 20% for 20 wt% BR. However, the measured heats of polymerization exceed the expected values, which is indicative of crosslinking between MIST and BR. For MIST formulations containing aliphatic maleimides (MIST1–3), this decrease is larger if 10 wt% BR is added to pure MIST for the first time than if the same amount of BR is added to increase BR content from 10 to 20 wt%. However, the opposite is the case for MIST4 containing the aromatic maleimide. Indeed, the underproportional decline of polymerization heat in formulations containing aliphatic maleimides exhibits a trend of decreasing underproportionality (MIST1 < MIST2 < MIST3). The inversion of this trend for the least reactive formulation containing the aromatic maleimide (MIST4) is the logical extension. This observation reveals that the influence of BR addition on inter-phase crosslinking is lower for faster and more reactive systems. Interestingly, there is no trend visible for the development of polymerization heat of the reference IBMA with BR concentration increase. This reflects the contradiction of polymerization speed and overall reactivity of this formulation compared to MIST formulations.

RT-NIR-photoreology studies were further used to characterize DBC of the resulting crosslinked polymers (Table 3, Fig. 3). As expected, DBC until gelation drops with increasing BR content in all cases due to increased viscosity. Analogously, reaction times until 95% conversion increase with increasing BR content. Interestingly, however, the final DBC increases for increasing BR content for MIST-based polymers, while it remains constant for IBMA-based reference polymers. This may be explained by stronger Trommsdorff effects at higher BR contents as radical destruction decreases due to gelling while monomers remain mobile and continue to react. Shrinkage forces were higher for more BR content with the exception of MIST1. All of these observations are

Table 4. Summary of obtained thermomechanical properties of materials from formulations MIST1–3 without and with 10 or 20 wt% poly(butadiene) (BR) and of hot-pressed ABS (FDM filament) during tensile testing (stress at break σ , strain at break ϵ), Dynstat (impact resistance r) and DMTA (shear modulus $G'_{25^\circ\text{C}}$, glass transition temperature T_g) experiments

| Polymer ^a | σ / MPa | ϵ / % | r / kJ m ⁻² | $G'_{25^\circ\text{C}}$ / GPa | T_g / °C ^b |
|----------------------|----------------|----------------|--------------------------|-------------------------------|-------------------------|
| pMIST1_0 | 27.5 ± 3.0 | 4.3 ± 0.7 | 1.8 ± 0.50 | 1.26 | 163 |
| pMIST1_10 | 22.0 ± 2.5 | 45.6 ± 7.0 | n.d. ^c | 0.21 | −98; 40; 184 |
| pMIST1_20 | 12.4 ± 0.6 | 54.6 ± 3.9 | n.d. ^c | 0.062 | −97; 33; 192 |
| pMIST2_0 | 8.0 ± 1.1 | 1.1 ± 0.3 | 0.4 ± 0.2 | 0.67 | 94 |
| pMIST2_10 | 9.4 ± 0.4 | 6.0 ± 0.0 | 6.8 ± 1.9 ^d | 0.23 | −96; 33; 94 |
| pMIST2_20 | 6.5 ± 0.6 | 122.9 ± 31.7 | n.d. ^c | 0.068 | −84; 33; 94 |
| pMIST3_0 | 3.0 ± 0.2 | 1.3 ± 0.3 | 0.5 ± 0.2 | 1.22 | 173 |
| pMIST3_10 | 5.0 ± 0.2 | 1.9 ± 0.2 | 1.4 ± 0.5 | 0.51 | −95; 83; 173 |
| pMIST3_20 | 6.4 ± 0.4 | 6.2 ± 1.6 | 15.9 ± 6.4 ^d | 0.21 | −97; 83; 159 |
| ABS | 32.6 ± 0.2 | 14 ± 3 | 47.0 ^d | 0.59 | ≥120 |

^a Each polymer contains equimolar amounts of maleimide (MI) and styrene (St) monomers, where the numbers 1–3 characterize the MI/St combination according to Scheme 1; the number at the end describes the content of poly(butadiene) rubber (BR, 180 kDa) in wt%, i.e. 0 wt%, 10 wt% or 20 wt%.

^b Determined from the maxima of the loss modulus curves; formulations containing 10 or 20 wt% BR: lowest T_g is attributed to BR, highest T_g to MIST and middle T_g to mixed phase of BR and MIST.

^c Did not break with 4 J hammer (equivalent to 100 kJ m⁻²).

^d Hinge break with 4 J hammer (equivalent to 100 kJ m⁻²).

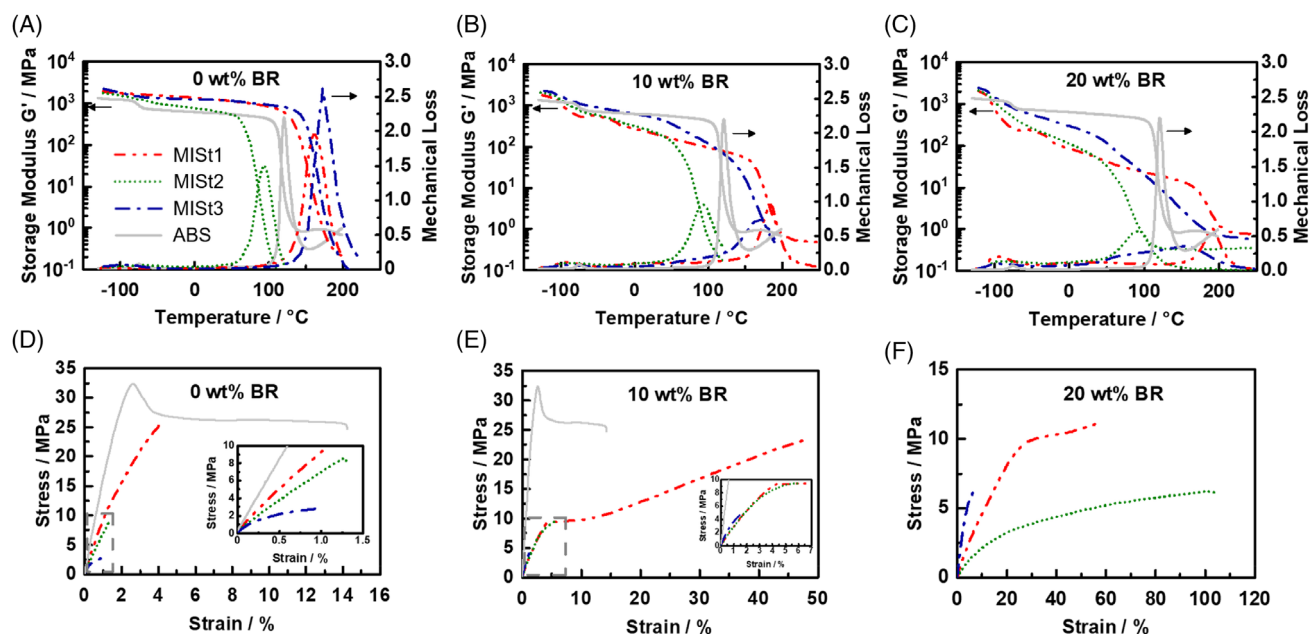


Figure 4. DMTA curves for pMIST1–3 ((A)–(C)) and representative tensile test results for pMIST1–3 ((D)–(F)) with 0, 10 and 20 wt% poly(butadiene) rubber (BR).

consistent with the result that inter-phase crosslinking is higher for less reactive MIST systems.

To further confirm the changes in crosslinking behavior upon BR addition, swelling experiments were also conducted for BR-containing photopolymers (Table 2). While swellability studies of pure pMIST polymers had shown that MIST1-, MIST2- and MIST3-based polymers were already crosslinked previously to BR addition, swellability studies with BR-containing polymers showed that the previously un-crosslinked MIST4-based polymer crosslinked upon BR addition. Furthermore, swellability studies of pMIST_0, pMIST_10 and pMIST_20 polymers (for MIST1–4) showed that swelling decreased with increasing BR content, especially for pMIST2- and pMIST3-based systems. These results clearly

indicate that BR is covalently included in the polymer network via its double bonds. The increase in gel fractions with higher BR contents furthermore confirms the higher DBC at higher BR contents found during RT-NIR-photocrosslinking.

Covalent linkages between MIST and BR may aid mimicry of ABS, in which poly(styrene-co-acrylonitrile) is grafted onto poly(butadiene) chains in most materials of this type. However, high crosslinking densities will counteract potential phase separation, which influences the mechanical performance significantly as corroborated by the varying mechanical performance of different ABS types due to their distinct microphase structures. Therefore, formulations with varying BR content were characterized with respect to their (thermo)mechanical performance for more

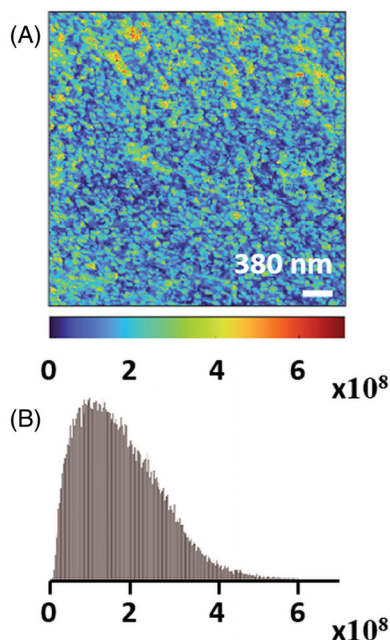


Figure 5. Indentation moduli as determined by AFM of pMIS2 with 10 wt % poly(butadiene) rubber (BR). (A) shows a $5 \times 5 \mu\text{m}^2$ area with indentation force corresponding color bars in Pa and a white scale bar corresponding to 380 nm. (B) shows the determined indentation moduli histogram for (A).

information on their microphase separation behavior (Table 4, Fig. 4).

Toughening with poly(butadiene) rubber: material properties

Thermal and mechanical properties were examined to study toughening more closely for materials containing aliphatic maleimide substituents (pMIS1–3). Here it must be mentioned that the

irradiation conditions of the utilized curing oven provided higher intensities than the conditions for photo-DSC and photo-rheological studies previously, as the light sources had to be coupled into light guides. The low final conversion of materials with aromatic maleimide substitution (pMIS4) in combination with their inability to crosslink the MIS and BR component resulted in flexible but not tough materials. Therefore, they were excluded from further testing.

To test the thermal range in which DMTA could be performed, thermal stability of the materials was evaluated by simultaneous thermal analysis (Table S3). The trends of heat stability follow the usual influence of maleimide *N* substitution and BR addition. Stability increases for increasing BR addition, i.e. crosslinking, and decreases for increasing steric hindrance, i.e. decreasing inter-phase crosslinking ability. Notably, pMIS1 without BR still exceeds the thermal stability of ABS (418 °C versus 406 °C) while pMIS2 and pMIS3 are of the same order of magnitude as ABS. All BR-containing polymers of MIS1–3 exhibit enhanced thermal stability compared to ABS.

DMTA confirmed incomplete miscibility of BR and MIS in all materials since two glass transitions for the two constituents, the MIS copolymer (94–192 °C) and BR (–98 to –84 °C), are present in the loss modulus curves of pMIS₁₀ and pMIS₂₀ (Table 4, Figs 4(A)–4(C)). Compatibility increases with increasing BR content due to the crosslinks between the components, which becomes evident with emerging new maxima in the loss factor curve between the two original glass transition temperatures (33–83 °C). These new signals are only slightly visible at 10 wt% BR content (Fig. 4(B)) and become more pronounced at 20 wt% (Fig. 4(C)). The strong influence of the maleimide *N* substituents on material properties is also evident in DMTA. First, the relative positioning of the glass transition (T_g) is largely dependent on it. The rigid cyclohexyl moiety in pMIS3 increases T_g , slightly (173 °C) compared to *N*-propyl substituted pMIS1 (163 °C). T_g of pure pMIS2 is much lower (94 °C) due to the plasticizing nature of its longer *N*-alkyl chain substituent. These T_g values are

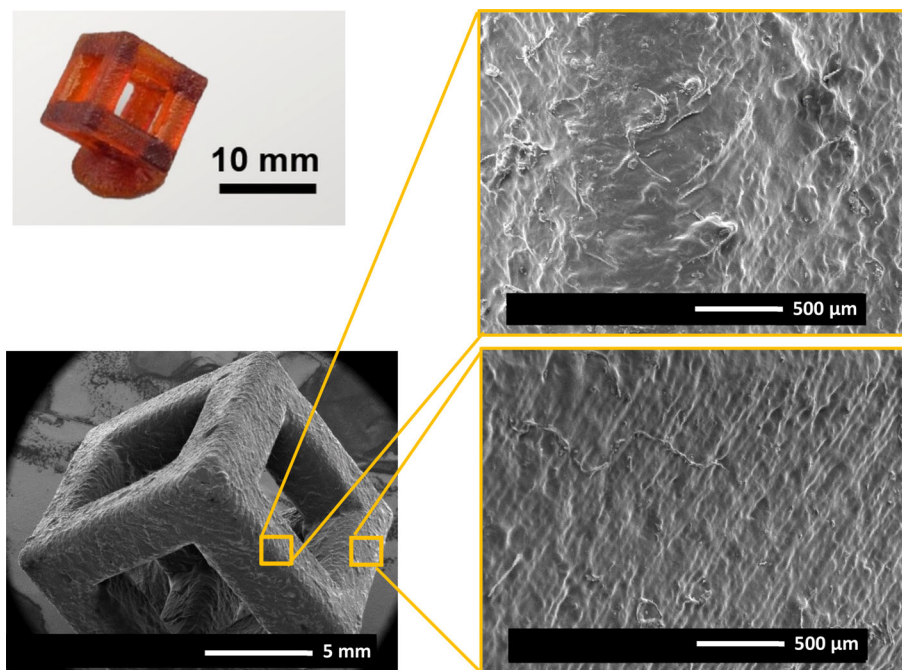


Figure 6. 3D structure printed from MIS2₁₀ and corresponding SEM images.

considerably higher than the T_g values of ABS (120 °C), with the exception of pMIST2. Second, the substituent influences the impact of BR addition on phase separation. Increasing amounts of BR cause the glass transition of the pure MIST phase in pMIST1 to increase (163 to 192 °C) while the T_g of pMIST2 remains unchanged for all BR contents (94 °C) and decreases for pMIST3 containing more BR (173 to 159 °C) (Table 4). This trend reflects a lower tendency of materials containing bulkier maleimide N substituents to phase separate, which is consistent with the crosslinking behavior between MIST and BR observed during swelling experiments (Table 2, grey entries). Crosslinking densities increase drastically from pure MIST2 and MIST3 formulations (swellabilities of $ca\ 10^4\%$) to MIST formulations containing 10 wt% BR ($ca\ 10^3\%$), while only a marginal increase is observed from 10 to 20 wt% BR content (swellability decreases within the same order of magnitude). The MIST1-based polymer without BR, however, exhibits already a swellability of only $ca\ 10^3\%$, which is within the same order of magnitude of BR-containing MIST1–3 polymers. This advocates for higher crosslinking between the BR and MIST system compared to crosslinking within the MIST phase for sterically demanding pMIST2 and pMIST3, i.e. lower phase separation, as opposed to PrMI-based pMIST1.

Furthermore, DMTA showed that increasing BR contents decrease the storage modulus at room temperature in all materials as expected. pMIST3 maintains a higher storage modulus at room temperature upon BR addition compared to pMIST1 and pMIST2 due to the rigid cycloaliphatic substituent (Figs 4(A)–4(C)). pMIST2 shows a much lower storage modulus compared to pMIST1 and pMIST3 (Fig. 4(A)), which seems to get lost upon BR addition (Figs 4(B), 4(C)). This confirms the plasticizing effect of the N -alkyl side chain as described during T_g evaluation.

Tensile tests and Dynstat impact resistance experiments show that BR increases toughness for all materials (Table 4, Figs 4(D)–4(F)). Upon increase of BR content from 10 to 20 wt%, rubbery behavior already dominates the material properties and ultimate tensile stress values and Young's moduli decrease strongly. As expected, MIST1- and MIST2-based materials with linear aliphatic substituents are tougher than MIST3-based materials with more rigid cyclohexane substituents.

MIST1-based materials exhibit the highest ultimate tensile strengths. This can be explained by their small propyl substituents of the maleimide and lower inter-phase crosslinking, which allow for better phase separation as indicated in DMTA experiments. The strength of pMIST1_0 without BR toughening almost reaches the yield stress of an ABS filament for FDM (27.5 versus 32.6 MPa, Fig. 4(D), Table 4). However, as expected, it is much more brittle than ABS (4.3% versus 14% elongation at break, Fig. 4(D)). The more flexible nature of pMIST1_10 compared to the ABS filament is reflected in the lower maximum stress (22.0 MPa) and shear modulus (0.21 GPa) as well as the higher elongation at break (45.6%) (Fig. 4(E), Table 4). Contrary to brittle pMIST1_0, pMIST1_10's impact resistance is higher than that of the ABS filament. While the pMIST1_10 specimen did not break with the 4 J hammer and stopped the motion of the hammer almost completely during Dynstat without the occurrence of a crack or other visible damage (estimated impact resistance $\geq 100\text{ kJ m}^{-2}$), the ABS specimen broke incompletely with visible stress whitening (estimated impact resistance $ca\ 47.0\text{ kJ m}^{-2}$). This is especially remarkable if pMIST1_10's T_g of 184 °C compared to the T_g of 120 °C for the ABS filament is considered.

Longer linear aliphatic substituents in MIST2-based polymers decrease the mechanical performance as well as the glass

transition temperature due to their plasticizing effect. This seems to be an unavoidable trade-off for lower volatility of the corresponding monomers. Nonetheless, the improvement of impact resistance upon addition of 10 or 20 wt% BR demonstrates the feasibility of the developed toughening strategy for photopolymers.

Analysis of phase separation in MIST2_10

While bulk material analyses clearly indicate phase separation between MIST and the rubber, the materials' transparent appearance is counterintuitive to this result. In transparent materials, phase separation can only occur if the domain sizes are below the wavelength of visible light ($<380\text{ nm}$). Therefore, the degree and dimensions of phase separation were characterized through locally resolved mechanical analysis via AFM nanoindentation experiments for pMIST2_10, which was 3D printed in the end.

The resulting indentation modulus image indicates phase separation with domain sizes below 100 nm (Fig. 5(A)). The corresponding histogram (Fig. 5(B)) cannot fully resolve the bimodal nature of the two phases due to the closeness of the indentation moduli of the hard and soft phases. This may be a result of sample preparation to obtain even enough surfaces for the measurements. Peak deconvolution suggests maxima at approximately 0.1 GPa and 0.3 GPa, which should be interpreted cautiously due to the necessary sample preparation.

In conformity with AFM analysis, SAXS reveals similar results for the particle size of the randomly spherical distributed elastomers in the matrix (estimated spherical scatterer size of 78.34 nm). Details regarding the analysis can be found in the Supplementary information.

3D printing of MIST2_10

While MIST1 performed best mechanically, its monomers are too volatile for 3D printing (Table S1). Therefore, the mechanically second-best performing material MIST2 was identified as the ideal formulation for DLP printing. Its longer aliphatic maleimide substituent results in lower volatility (Table S1) yet good chemical reactivity and acceptable viscosity (Table S2). 10 wt% BR content was chosen due to the resulting material's tough but not yet elastomeric mechanical performance. The printing parameters were determined from exposure studies and subsequent printing of a complex $8 \times 8 \times 8\text{ mm}^3$ hollow cube structure was possible (Fig. 6). Already without highly specific process optimization the results are very promising. The overall shape of the cube is already satisfactory and the details of the edge region and of a flat side wall show a dense, well-connected surface in SEM images.

CONCLUSION

This work developed and characterized a photopolymerizable system with various maleimides, substituted styrenes and BR, in which BR was utilized as a toughening component in the terpolymer similarly to ABS. MIST4, which contains aromatically substituted maleimide, was too unreactive to achieve appropriate conversions while all systems based on aliphatically substituted maleimides (MIST1–3) reached above 90% DBC. Overall, more effective photopolymerization was achieved for all MIST monomer systems compared to the standard methacrylic monomer IBMA. Crosslinking between BR and the maleimide–styrene copolymer as well as variation of the maleimide N substituent were investigated to assess their impact on (thermo)mechanical properties as well as on phase separation. The presence of phase separation

despite the transparent appearance of the materials was proved by DMTA, AFM nanoindentation and SAXS. It was shown that phase separation can be influenced through maleimide *N* substituents and BR content. As a result, the new monomer system of maleimide, styrene and BR is tunable for photopolymerization in many application fields where tough, ABS-imitating photopolymers are needed by simply adjusting the maleimide and styrene substituents and the BR content of the formulation. With the exception of the MIST3-based polymer, all obtained polymers were either thermally equally stable (MIST2_0-based polymer) or more stable than ABS (all other MIST-based polymers) with T_g values up to 190 °C. The mechanically best performing polymer pMIST1_10, consisting of equimolar amounts of PrMI and tBuSt, and 10 wt% BR, reaches lower tensile strength and shear modulus but higher elongation at break and impact resistance than an ABS filament for FDM. Since its components are too volatile for 3D printing, the less volatile yet tough MIST2_10 formulation containing EHMI, FES and 10 wt% BR was chosen for 3D processing and proved to be well printable. Therefore, we were able to demonstrate that the use of high molecular weight rubbers is a cheap and robust toughening strategy for photopolymers intended for AM of ABS-inspired materials.

ACKNOWLEDGEMENTS

We thank FWF for their funding (P27059 'Advanced toughening concepts for 3D-printable photopolymers'). BUNA CB24 (a >96% *cis*-1,4-poly(butadiene)) was kindly gifted from Arlanxeo. The photoinitiators Ivocerin and ethyl (2,4,6-trimethylbenzoyl) phenyl (TPO-L) were kindly gifted by Ivoclar Vivadent and Lambson, respectively.

REFERENCES

- Ligon SC, Liska R, Stampfl J, Gurr M and Mulhaupt R, *Chem Rev* **117**: 10212–10290 (2017).
- Stansbury JW and Idacavage MJ, *Dent Mater* **32**:54–64 (2016).
- Ligon-Auer SC, Schwentenwein M, Gorsche C, Stampfl J and Liska R, *Polym Chem* **7**:257–286 (2016).
- Kade MJ, Burke DJ and Hawker CJ, *J Polym Sci A Polym Chem* **48**:743–750 (2010).
- Hoyle CE and Bowman CN, *Angew Chem Int Ed* **49**:1540–1573 (2010).
- Oesterreicher A, Gorsche C, Ayalur-Karunakaran S, Moser A, Edler M, Pinter G et al., *Macromol Rapid Commun* **37**:1701–1706 (2016).
- Matyjaszewski K and Spanswick J, *Mater Today* **8**:26–33 (2005).
- Georges MK, Veregin RPN, Kazmaier PM and Hamer GK, *Macromolecules* **26**:2987–2988 (1993).
- Hawker CJ, Bosman AW and Harth E, *Chem Rev* **101**:3661–3688 (2001).
- Meijs GF, Rizzardo E and Thang SH, *Macromolecules* **21**:3122–3124 (1988).
- Gorsche C, Seidler K, Knaack P, Dorfinger P, Koch T, Stampfl J et al., *Polym Chem* **7**:2009–2014 (2016).
- Gorsche C, Seidler K, Harikrishna R, Kury M, Koch T, Moszner N et al., *Polymer* **158**:149–157 (2018).
- Gauss P, Ligon-Auer SC, Griesser M, Gorsche C, Svajdlenkova H, Koch T et al., *J Polym Sci A Polym Chem* **54**:1417–1427 (2016).
- Phommalsack-Lovan J, Chu Y, Boyer C and Xu J, *Chem Commun* **54**: 6591–6606 (2018).
- Fenoli CR, Wydra JW and Bowman CN, *Macromolecules* **47**:907–915 (2014).
- Ribelli TG, Konkolewicz D, Bernhard S and Matyjaszewski K, *J Am Chem Soc* **136**:13303–13312 (2014).
- Leibfarth FA, Mattson KM, Fors BP, Collins HA and Hawker CJ, *Angew Chem Int Ed Engl* **52**:199–210 (2013).
- Ning N, Liu W, Hu Q, Zhang L, Jiang Q, Qiu Y et al., *Composit Sci Technol* **199**:108364 (2020).
- Hazot P, Pichot C and Maazouz A, *Macromol Chem Phys* **201**:632–641 (2000).
- Pearson RA and Yee AF, *J Mater Sci* **26**:3828–3844 (1991).
- Robinette EJ, Ziaee S and Palmese GR, *Polymer* **45**:6143–6154 (2004).
- Auad ML, Frontini PM, Borrajo J and Aranguren MI, *Polymer* **42**:3723–3730 (2001).
- Ullett JS and Chartoff RP, *Polym Eng Sci* **35**:1086–1097 (1995).
- J. Ebert and R. Gmeiner, *Stereolithography Device Having a Heating Unit* (2020).
- Steyrer B, Buseti B, Harakaly G, Liska R and Stampfl J, *Addit Manuf* **21**: 209–214 (2018).
- Strong AB, Thermoplastic materials (commodity plastics), in *Plastics: Materials and Processing*, ed. by Yarnell D. Prentice Hal, Hoboken, NJ, p. 251 (2006).
- G. H. Fremon and W. N. Stoops, Shock resistant compositions prepared by polymerizing styrene and acrylonitrile with polybutadiene. US Patent US3168593 (1965).
- Herzberger J, Sirrine JM, Williams CB and Long TE, *Prog Polym Sci* **97**:1–44 (2019).
- Popescu D, Zapciu A, Amza C, Baciu F and Marinescu R, *Polym Test* **69**: 157–166 (2018).
- Dolci E, Froidevaux V, Joly-Duhamel C, Auvergne R, Boutevin B and Caillol S, *Polym Rev* **56**:512–556 (2016).
- Ke L, Hu D, Lu Y, Feng S, Xie Y and Xu W, *Polym Degrad Stab* **97**:132–138 (2012).
- Moore ER and Pickelman DM, *Ind Eng Chem Prod Res Dev* **25**:603–609 (1986).
- Oswal S, Bhandari VK, Bhamore P and Malek NI, *Int J Polym Mater* **56**: 421–435 (2007).
- Gorsche C, Harikrishna R, Baudis S, Knaack P, Husar B, Laeuger J et al., *Anal Chem* **89**:4958–4968 (2017).
- Hutter JL and Bechhoefer J, *Rev Sci Instrum* **64**:1868–1873 (1993).
- Andriotis OG, Manuyakorn W, Zekonyte J, Katsamenis OL, Fabri S, Howarth PH et al., *J Mech Behav Biomed Mater* **39**:9–26 (2014).
- Fischer-Cripps AC, *Nanoindentation*. Springer, New York, NY (2002).
- Joensson S, Viswanathan K, Hoyle CE, Clark SC, Miller C, Nguyen C et al., *J Photopolym Sci Technol* **13**:125–143 (2000).
- Hoyle CE, Clark SC, Jonsson S and Shimose M, *Polymer* **38**:5695–5697 (1997).
- Bonneaud C, Burgess JM, Bongiovanni R, Joly-Duhamel C and Friesen CM, *J Polym Sci A Polym Chem* **57**:699–707 (2019).
- Yamazaki H, Matsumoto A and Otsu T, *Eur Polym J* **33**:157–162 (1997).
- Oishi T, Kagawa K and Nagata H, *Polymer* **38**:1461–1469 (1997).